

Connecting low-energy orbits in the Saturn system

Normal Paper

Elena Fantino¹, Elisa Maria Alessi^{2,1} and Jesús Peláez³

¹ Department of Aerospace Engineering, Khalifa University of Science and Technology, P.O. Box 127788, Abu Dhabi, United Arab Emirates

² Istituto di Fisica Applicata "Nello Carrara", Consiglio Nazionale delle Ricerche, via Madonna del Piano 10, 50019 Sesto Fiorentino (FI), Italy

³ Space Dynamics Group, School of Aeronautical and Space Engineering, Technical University of Madrid, Plaza Cardenal Cisneros 3, 28040 Madrid, Spain

Abstract

Based on Cassini's findings, scientists think that the Saturn system is home to multiple moons that could be hospitable to life. This has given impulse to several mission proposals and to investigations on new, efficient and effective ways to reach and explore the major moons of Saturn and the ring system. The bulk of the proposed solutions is based on the patched conics technique, implying fast approaches with low ΔV requirements and involving use of chemical propulsion. A trajectory designed with the low-energy orbits of the three-body problems of Saturn and each of its Inner Large Moons (Mimas, Enceladus, Tethys, Dione) offers interesting alternative observation scenarios. In this work, the case of planar Lyapunov orbits is analysed for the purpose. Their hyperbolic invariant manifolds are used to connect consecutive moons. However, since these objects do not overlap in configuration space, a strategy based on low-thrust maneuvers is developed, and preliminary results are presented. With a continuous thrust of 25 mN magnitude, it is possible to connect Tethys and Dione in just 50 days using 9 kg of propellant. The needed power can be provided by three radioisotope thermoelectric generators.

Keywords: circular restricted three-body problem, planar Lyapunov orbits, hyperbolic invariant manifolds, low-thrust transfers, Saturn moons

1. Introduction

In the framework of the future generation of solar system exploration missions, high priority is given to the observation of the so-called Inner Large Moons of Saturn, namely, Mimas, Enceladus, Tethys and Dione (see Table 1), which are closely related to the E-ring. In particular, Enceladus is considered the main source of its replenishment. For the ascertained presence of liquid water, which likely extends beneath its entire surface, Enceladus is considered the first target to search for life and analyse habitability features [1][2]. Moreover, due to the observed cryovolcanism and tectonics, the scientific community looks at Enceladus as the key to explain the evolution of other icy satellites not only in the Saturn system, but also in the Jupiter and Uranus systems [3]. As detailed in [4][5], the *Cassini* mission fulfilled many of the goals established since its conception, but it also brought new challenges regarding the Inner Large Moons, which are all icy bodies. For instance, dynamical models of Mimas and Dione indicate the existence of an ocean beneath their surface, but a full evidence for that is still missing. Moreover, the origin of the red streaks on Tethys is under debate, and so is the alleged young origin of the moons in relation with the dense cratering features. Other scientific open questions regard the moons relative orbital dynamics, their surface composition, and the thermal and internal activity.

The proposed mission concepts for the exploration of, e.g., Enceladus rely on two main dynamical approaches: the design of stable orbits around Enceladus [6] and the design of flybys at the moon satisfying certain observational constraints [7][8][2]. In the latter category, the so-called *resonant hopping* tours are conceived as sequences of orbits in mean motion resonance

with the moon, and the periodic perturbation caused by the moon is exploited to change the planetocentric trajectory conveniently. The initial design performed under Keplerian approximation can be refined within the Circular Restricted Three-Body Problem (CR3BP) (see, e.g., [9]). In [10], different options are analysed, in particular mean motion resonant orbits with Enceladus but also Libration Point Orbits (LPOs) in the Saturn-Enceladus system. The same author finds support to the use of this dynamical model in the observational proof of the existence of Trojans in the Saturn-Dione and the Saturn-Tethys systems.

In this work, we propose trajectories to connect Mimas, Enceladus, Tethys and Dione, based on the dynamics of LPOs and on the use of low-thrust propulsion. The low eccentricities of the lunar orbits justify the assumption of circular motion around Saturn and the adoption of the CR3BP as a dynamical model for the design of the trajectory of the spacecraft. The low inclination with respect to the common reference plane supports the approximation that the lunar orbits are coplanar, a fact exploited in the adopted 2D approach. The start and end of each transfer is a planar Lyapunov orbit (PLO) around either L_1 or L_2 of a Saturn-moon CR3BP. PLOs can be used as science orbits, a choice which guarantees time-flexibility (a PLO is periodic) while offering uninterrupted view of the moon at low relative speeds. The transfer between consecutive moons is initialised at appropriate states obtained by Keplerian approximation of the hyperbolic stable/unstable hyperbolic invariant manifolds (HIMs) of the PLOs and then achieved by means of electric propulsion. A similar concept can be found in [11] regarding transfers from Oberon to Miranda in the Uranus system: optimal low-thrust arcs connect hyperbolic invariant manifolds of libration points of consecutive CR3BPs, the required electrical power being provided by one Radioisotope Thermoelectric Generator (RTG). Heteroclinic connections were computed to move from L_2 to L_1 . The idea of using RTGs to propel a spacecraft to the outer planets is becoming more and more common. The readers are referred to [12] for an application of this technology to a Neptune exploration mission.

The paper is organised as follows: Section 2 defines the dynamical model, presents the families of PLOs around L_1 and L_2 of Dione, Tethys, Enceladus and Mimas and describes the 2-body model applied to their HIMs. Section 3 illustrates the moon-to-moon transfer strategy, the results of which are discussed in Section 4 and 5. Abbreviations found in tables and figures are defined as follows: S = Saturn, Di = Dione, Te = Tethys, En = Enceladus, Mi = Mimas.

Table 1. Mass (second column), physical radius (third column) and basic orbital data (columns four to seven) of the four Inner Large Moons of Saturn.

Moon	Mass (10^{19} kg)	Mean radius (km)	Inclination (degrees)	Period (days)	Semimajor axis (km)	Eccentricity
Dione	109.57	561	0.028	2.737	377415	0.0022
Tethys	61.76	533	1.091	1.888	294672	0.0001
Enceladus	10.79	252	0.003	1.370	238042	0.0000
Mimas	3.75	198	1.574	0.942	185539	0.0196

Mass of Saturn $M_s = 5.68336 \cdot 10^{26}$ kg

2. The dynamical model

The CR3BP [11] models the motion of a massless body subjected to the gravitational attraction of two primaries of mass m_1 and m_2 on circular orbits around their common centre of mass. The equations of motion are referred to the barycentric synodical reference frame, on the x -axis of which the primaries occupy fixed positions. A normalized system of units is adopted by assigning unit value to the gravitational constant, to the sum (m_1+m_2) of the masses of the primaries and to their distance r_{12} . Then, as a result of Kepler's third law, the mutual orbital mean motion n_{12} equals 1, which defines the unit of time.

The dynamical system is characterized by one parameter, the mass ratio $\mu = m_2 / (m_1 + m_2)$, i.e., the mass of the second primary in normalized units. The more massive primary (here Saturn) lies at $(\mu, 0, 0)$ whereas the moon is at $(-1 + \mu, 0, 0)$. In this work, the trajectory of the third body is assumed to be contained in the xy -plane of the system. The CR3BP admits one integral of

motion - the Jacobi constant C_J - which is related to the mechanical energy E of the third body in the synodical frame ($C_J = -2E$). Five equilibrium points, denoted L_i , $i=1,2,\dots,5$, further characterize the system, the first three - the so-called collinear points - lying on the x -axis at positions which depend on the value of μ , and the remaining two forming equilateral triangles with the primaries. In the following, we focus on the dynamics in the neighbourhood of L_1 and L_2 : L_1 is between the moon and Saturn, L_2 on the opposite side with respect to the moon. Table 2 reports the basic features of the four CR3BPs considered in this work, i.e., the systems formed by Saturn and Dione, Tethys, Enceladus and Mimas, respectively. We display the value of μ , the units of distance U_d and time U_t , and the x -coordinates of L_1 and L_2 .

Planar Lyapunov orbits

The linear approximation of the equations of motion close to L_1 and L_2 leads to families of periodic orbits, in particular the planar Lyapunov orbits [14]. Given L_i ($j=1,2$), the initial state on a PLO can be approximated starting from one of the eigenvalues and corresponding eigenvectors associated with the elliptic behaviour, and then refined and continued through a differential correction method. Figure 1 and Figure 2 show the orbits computed and used in this work: they have been selected by allowing for a minimum closest approach distance to the moon of 100 km. The maximum and minimum values of C_J for each family are listed in Table 3 (recall that the lower the C_J the higher the energy). Figure 3 and Figure 4 give the distances and speeds along the selected PLOs relative to the moon. In a reference frame centred at the moon and with fixed axes, the orbits follow a retrograde motion, like the planets when seen from the Earth.

Table 2. Mass parameter μ , unit of distance U_d , unit of time U_t , x -coordinates x_1 and x_2 of L_1 and L_2 for the systems considered.

CR3BP	μ (10^{-6})	U_d (km)	U_t (hours)	x_1 (U_d)	x_2 (U_d)
SDi	1.93	377415	10.5	-0.99139329	1.00865250
STe	1.09	294672	7.2	-0.99288765	1.00714405
SEn	0.19	238042	5.2	-0.99601953	1.00399068
SMi	0.07	185539	3.6	-0.99720063	1.00280447

Figure 1. Families of PLOs around L_1 and L_2 in the synodical barycentric reference frame. Normalized units. Left: Saturn-Dione CR3BP. Right: Saturn-Tethys CR3BP.

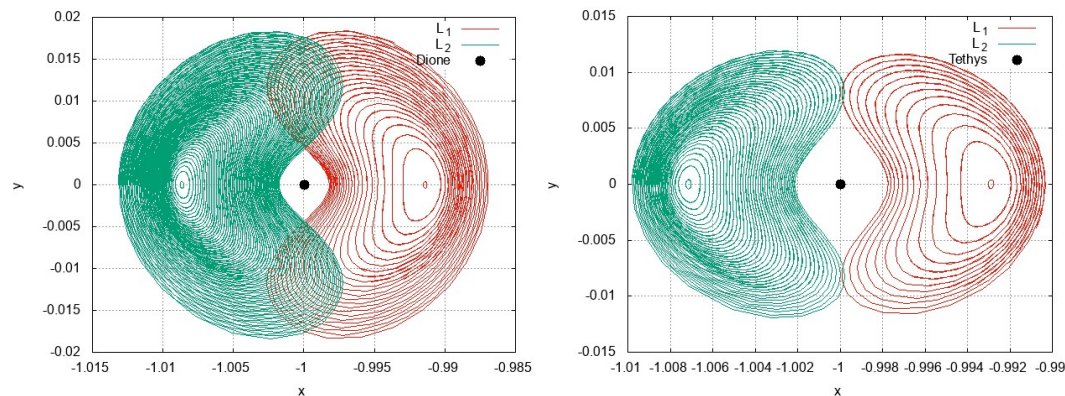


Figure 2. Families of PLOs around L_1 and L_2 in the synodical barycentric reference frame. Normalized units. Left: Saturn-Enceladus. Right: Saturn-Mimas.

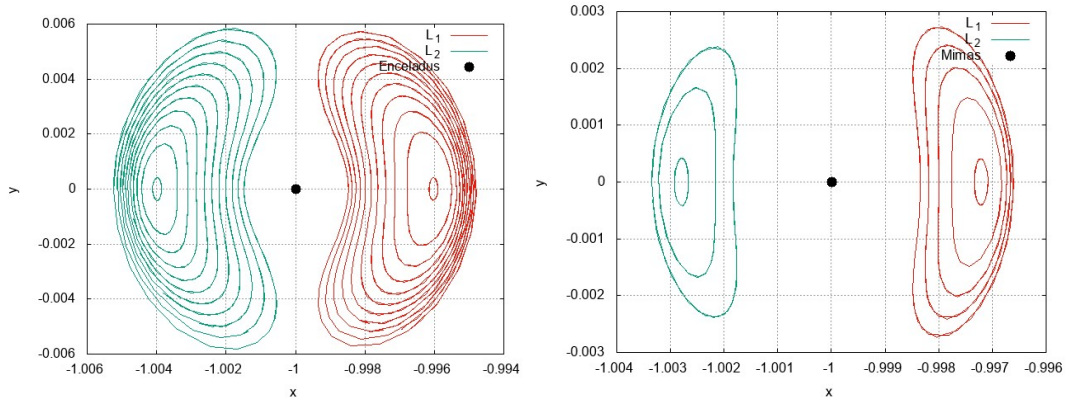


Table 3. Maximum and minimum values of C_J of the PLOs considered, respectively around L_1 and L_2 . The maximum y -amplitude and the maximum period over all the PLOs considered for a given Saturn-moon system are also reported.

CR3BP	$Max C_J (L_1)$	$Min C_J (L_1)$	$Max C_J (L_2)$	$Min C_J (L_2)$	$Max \Delta y (km)$	$Max T (days)$
SDi	3.00066516	3.00008008	3.00066259	3.00008109	6940	2.097
STe	3.00045419	3.00013242	3.00045273	3.00012420	3525	1.446
SEn	3.00014194	3.00005513	3.00014167	3.00005335	1391	0.839
SMi	3.00006993	3.00004688	3.00006981	3.00005205	506	0.497

Figure 3. Distance with respect to the given moon of the points on a given PLO, as a function of the C_J . From left to right: Saturn-Dione and Saturn-Tethys on the top; Saturn-Enceladus and Saturn-Mimas on the bottom.

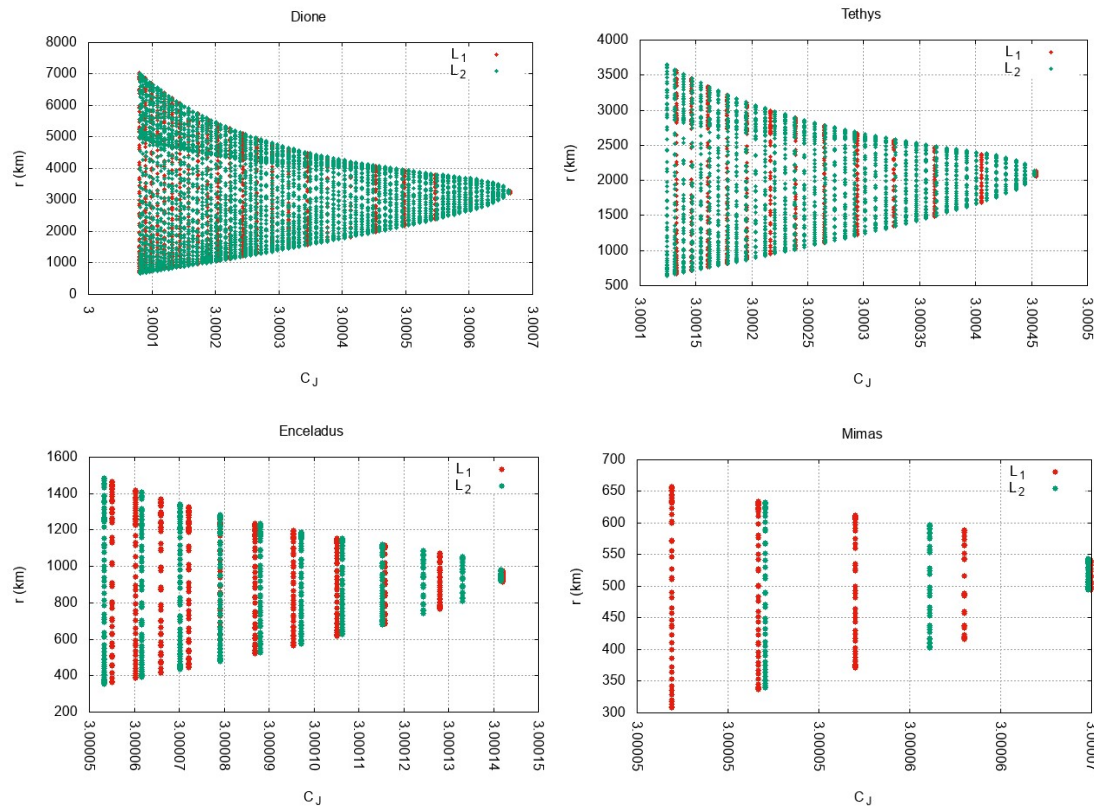
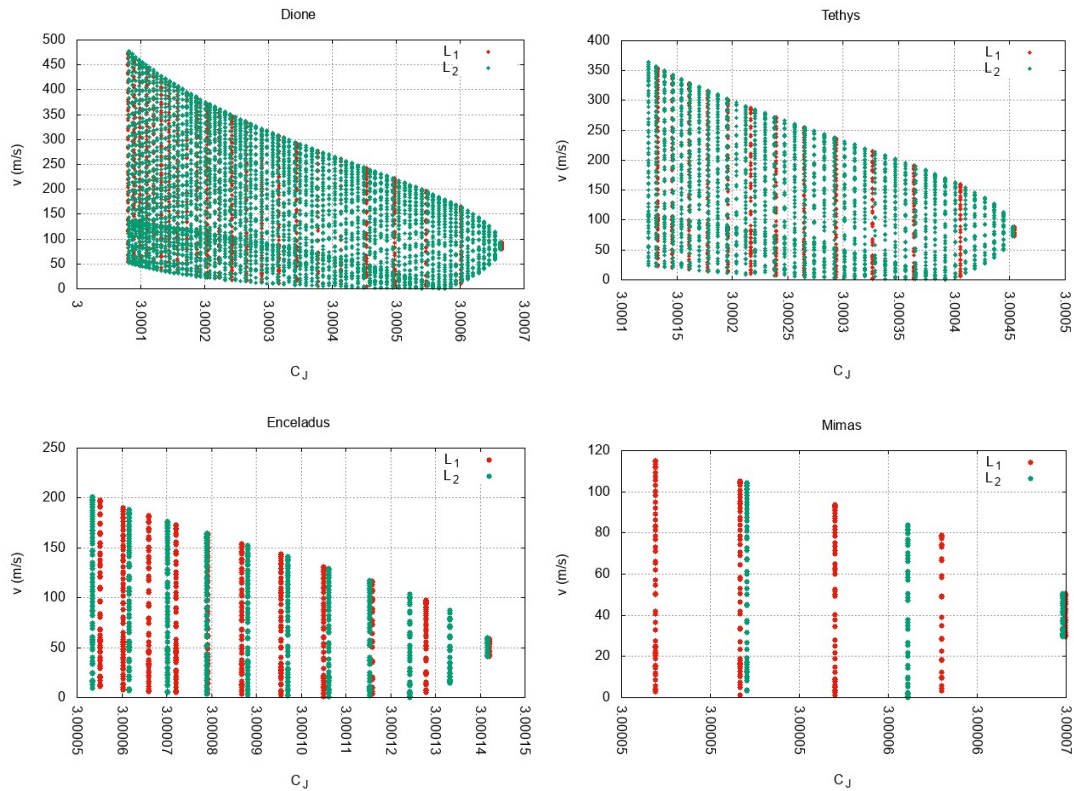


Figure 4. Speed relative to the moon on the PLOs (around L_1 and L_2 together) of the several families as a function of the Jacobi constant. Top left: Saturn-Dione. Top right: Saturn-Tethys. Bottom left: Saturn-Enceladus. Bottom right: Saturn-Mimas.



Hyperbolic invariant manifolds

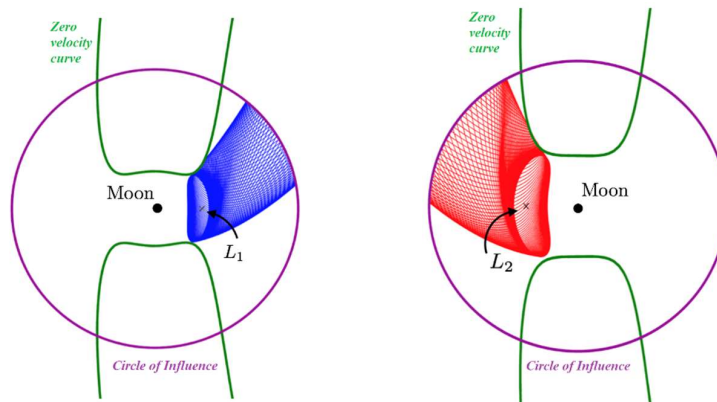
Appropriate branches of the stable and unstable hyperbolic invariant manifolds of the PLOs have been computed and propagated using standard methods, i.e., generating an initial state by applying a small perturbation in the direction of the stable/unstable eigenvector of the monodromy matrix of the PLO after appropriate time-transformation through the state transition matrix (see e.g., [15]). Each PLO is represented by 100 points, each of which constitutes the initial state of a HIM trajectory. The selected branches develop away from the moon (see Figure 5). Following [16], these trajectories are propagated up to a spherical surface of section (called circle of influence, CI) with centre at the moon and radius r_{CI} equal to n times the radius of the Laplace sphere r_{SOI} [17]:

$$r_{SOI} = r \left(\frac{m}{M_S} \right)^{2/5}, \quad (1)$$

where r and m are the moon's orbital radius and mass and M_S is the mass of Saturn (see Table 1).

The value of n is chosen in such a way that the CI includes all the PLOs of the family and cuts the flow of their HIMs transversally. In this work, $n = 4$ for all systems except for Saturn-Dione where $n = 5$. As a result, the radii of the 4 CIs are of 9768, 4851, 1951 and 996 km, respectively for Dione, Tethys, Enceladus and Mimas.

Figure 5. Examples of lunar CIs and a stable (left) and an unstable (right) HIM of PLOs around L_1 and L_2 , respectively.

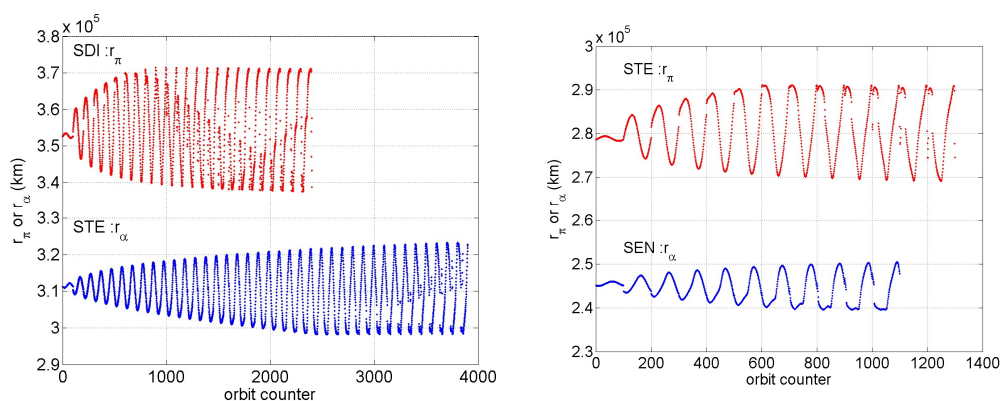


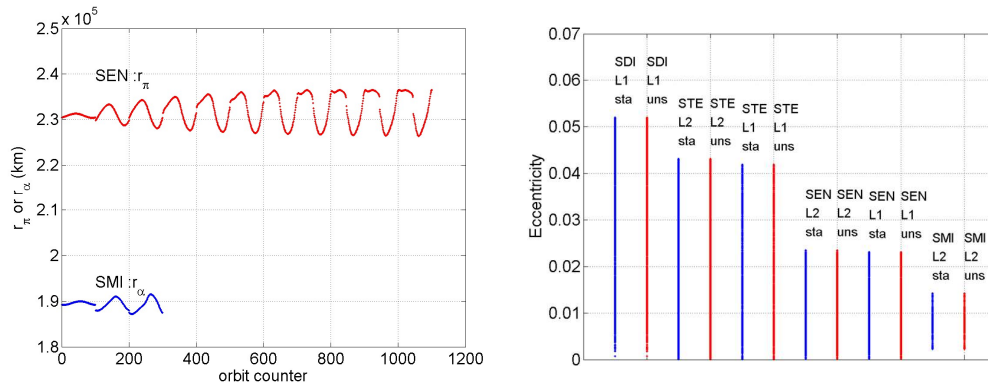
The authors in [16] showed that the error introduced by disregarding the gravity field of the moon at distances larger than r_{CI} is negligible ($< 1\%$ in terms of velocity magnitude). The states collected on the CI are represented in a planetocentric frame with fixed axes. These transformed states correspond to sets of osculating Keplerian orbital elements of elliptical orbits with focus at Saturn. Given the two-dimensional character of the solution, the only non-zero elements of each elliptical orbit are the semimajor axis a , the eccentricity e and the argument of the pericenter ω .

3. Moon-to-moon transfer strategy

The Keplerian approximation of the HIMs of the PLOs greatly simplifies the design of a low-energy (i.e., connecting states on low-energy orbits) transfer between consecutive moons. Such transfer takes place between a PLO around L_2 of the inner moon and a PLO around L_1 of the outer moon. The transfer direction (outward or inward) determines the stability character of the HIM to be employed at each end (unstable at departure, stable at arrival).

Figure 6. Comparison between pericenter and apocenter radii of the Keplerian approximations of HIM trajectories of PLOs at consecutive moons (top left: Dione-Tethys, top right: Tethys-Enceladus, bottom left: Enceladus-Mimas). The bottom right plot collects the values of the eccentricities of all the HIMs considered in this study, grouped on the basis of progenitor moon, equilibrium point and stability character.





The sets of orbital elements obtained with the method outlined above correspond to (coplanar) ellipses with focus at Saturn. These ellipses approximate the trajectories of the HIMs. Impulsive transfers between ellipses departing from the vicinity of a given moon and ellipses leading to the vicinity of a neighbouring moon can be easily computed analytically whenever the ellipses intersect each other. Note that the existence and position of the intersection point (i.e., the maneuver point) and the velocity difference ΔV between the two curves at the intersection point (i.e., the impulse to be provided by the onboard engine in order to move from one ellipse to the other and achieve the desired transfer) depend on the mutual orientation of the ellipses, expressed by the difference between the arguments of the pericenters of the two curves, which in turn is determined by the relative orbital phase of the progenitor moons. Such relative orbital phase provides a kinematic coupling between the two CR3BPs.

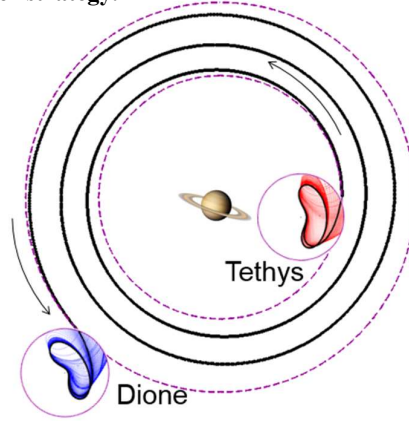
Now, the existence of such intersection requires that the apocenter of the ellipse of the inner CR3BP be higher than the pericenter of the ellipse of the outer CR3BP. Figure 6 shows that this never occurs for the transfers of this study, i.e., Dione-Tethys, Tethys-Enceladus, Enceladus-Mimas. This is due to the low eccentricities of the ellipses, meaning that the hyperbolic invariant manifolds of the LPOs of these moons follow almost circular paths in inertial space.

Under these circumstances, one could resort to a traditional, high-thrust Hohmann transfer. However, the cost of this option is extremely high, as shown by the performance analysis (time of flight ΔT_H , ΔV_H budget, propellant mass Δm_H) for the three transfers reported in Table 4 and obtained assuming a specific impulse of 300 s and spacecraft dry mass of 500 kg.

Table 4. Time of flight ΔT_H (second column), ΔV_H budget (third column), required propellant mass Δm_H (fourth column) of Hohmann transfers between consecutive moons (first column) with synodic period ΔT_s (fifth column). A spacecraft dry mass of 500 kg and a specific impulse of 300 s have been assumed.

Hohmann transfer	ΔT_H (hours)	ΔV_H (km/s)	Δm_H (kg)	ΔT_s (days)
Dione-Tethys	27.6	1.315	282	6.09
Tethys-Enceladus	19.5	1.274	271	0.50
Enceladus-Mimas	13.8	1.668	381	1.37

Figure 7. Sketch of the transfer strategy.



The strategy proposed here consists in using electric propulsion to perform circle-to-circle low- and continuous-thrust transfers between states at the CIs in a planetocentric, fixed-axes frame (Figure 7). These solutions constitute a first approximation to the computation of an optimal low-thrust transfer between ellipses, although taking into account the real eccentricities is not expected to bring remarkably different results. Note that under the assumption of continuous thrust, fuel and time optimality are simultaneously achieved on the tangential thrust solution. The ΔV_{LT} requirement is simply given by [18]:

$$\Delta V_{LT} = \sqrt{\frac{GM_S}{r_i}} - \sqrt{\frac{GM_S}{r_o}}, \quad (2)$$

being G the gravitational constant ($6.67259 \cdot 10^{-20} \text{ km}^3/\text{kg}/\text{s}^2$) and r_i and r_o the radii of the inner and outer circular orbits being connected. In the case of constant acceleration a_{LT} , the time of flight ΔT_{LT} is straightforwardly obtained from

$$\Delta T_{LT} = \Delta V_{LT}/a_{LT}. \quad (3)$$

The states selected to achieve a given transfer are those which minimize the cost among all the possible combinations of states at the two CIs.

4. Results

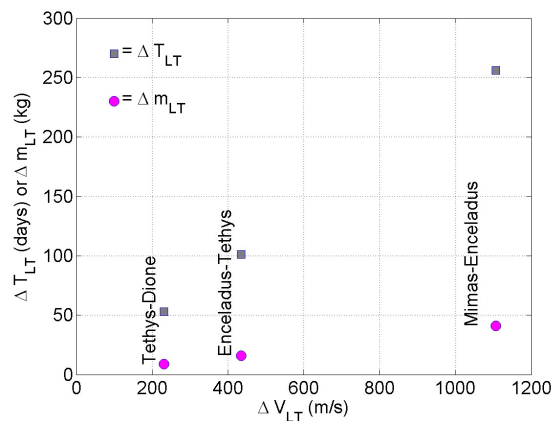
The low-thrust solutions obtained with the above method are described in Table 5 and in Figure 8. A spacecraft mass of 500 kg and a thrust of 25 mN provide an acceleration of $5 \cdot 10^{-8} \text{ km}/\text{s}^2$. This quantity has been assumed constant throughout the transfer. The propellant requirements have been computed using a flow rate of $1.85 \cdot 10^{-6} \text{ kg}/\text{s}$, as in the specifications of the NEXT ion thruster [19] for the above specified level of thrust. The times of flight reported in column 2 of Table 5 account only for the inter-CIs portion. The total transfer times between PLOs is obtained by adding the time taken to travel on the HIMs to/from the CIs. These times are of 1 day for Mimas and Enceladus, 2 days for Tethys and 4 days for Dione. For the sake of comparison, Table 5 also shows the performance of the circle-to-circle low-thrust transfers between (circular) lunar orbits with the same spacecraft mass and thrust (last three columns). The striking improvement both in terms of time of flight and propellant mass brought by the strategy here presented over the low-thrust transfer between lunar orbits is due to the fact that an appreciable fraction of the distance (and energy or velocity) gap between moons is covered by the invariant manifold trajectories. In other words, the perturbations caused by Saturn in the

vicinity of the moon (i.e., within its CI) drive the spacecraft away or towards the equilibrium point, and this in turns allows saving a non-negligible fraction of propellant mass.

Table 5. Time of flight ΔT_{LT} , ΔV_{LT} budget, required propellant mass Δm_{LT} of the low-energy circle-to-circle transfers between consecutive moons. The fifth, sixth and seventh columns show the time of flight ΔT_{LTm} and the velocity ΔV_{LTm} and mass Δm_{LTm} budgets for the circle-to-circle transfers between lunar orbits. The spacecraft mass is of 500 kg, the thrust provided is of 25 mN and the propellant flow rate is of $1.85 \cdot 10^{-6}$ kg/s.

Transfer	ΔT_{LT} (days)	ΔV_{LT} (km/s)	Δm_{LT} (kg)	ΔT_{LTm} (days)	ΔV_{LTm} (km/s)	Δm_{LTm} (kg)
Di-Te	53	0.231	9	306	1.320	49
Te-En	101	0.435	16	296	1.278	47
En-Mi	256	1.107	41	388	1.675	62

Figure 8. Performance of the selected low-thrust circle-to-circle transfers between CIs of consecutive moons: time of flight (ΔT_{LT}) and propellant mass (Δm_{LT}) versus velocity variation (ΔV_{LT}), propellant mass (Δm_{LT}) versus velocity variation (ΔV_{LT}).



5. Discussion and conclusions

In this work, low-thrust connections between low-energy states in two consecutive Saturn-moon CR3BPs have been computed and optimized assuming a simplified steering law, i.e., a continuous tangential thrust, to achieve optimal circle-to-circle transfers. The trajectory end states are the intersections between stable/unstable HIMs of PLOs of L_1 or L_2 with adequate surfaces of sections. The HIMs, in turn, lead or depart from the PLOs, which can serve as science orbits because they offer uninterrupted, low-relative speed views of the moons. For the chosen orbits, the maximum and minimum altitude where scientific observations can be achieved are in agreement with the ones corresponding to the fly-bys performed by *Cassini* at the same moons [5]. The distance to the lunar surface varies from a minimum of 100 km (fixed when selecting the PLOs) to a maximum of 460 km for Mimas, 1230 km for Enceladus, 3120 km for Tethys and 6480 km for Dione. These upper values correspond to the outermost (i.e., the biggest) PLOs in each family. In the case of Dione (the worst one), the spacecraft spends 5.5% of the PLO's period (about 3 hours) below an altitude of 1000 km.

The proposed transfer strategies require electric propulsion. Here we have referred to the NEXT ion thruster because it has been tested for continuous operation over 2.5 years and offers good performance features: at 25 mN of thrust it requires 600 W of input electrical power. The solar radiation flux at Saturn is extremely weak, so the propulsive system cannot run on photovoltaics. Nuclear energy such as that produced by an adequate number of RTGs is a good alternative, as this technology is well known and has flown on all deep space missions to the outer solar system. The standard RTG based on Pu^{238} has a mass of 55 kg and can provide 250 W of electrical power for several years. Hence, a suite of three such generators can power the propulsion system with little impact on the mass budget.

From the point of view of trajectory design, the periodic character of PLOs and the high degree of time flexibility of low-thrust transfers remove one intrinsic major constraint appearing when coupling CR3BPS, i.e., the need for time synchronization between the involved synodical reference frames: as a matter of fact, by introducing coast arcs during the moon-to-moon journeys, it is possible to increase the transfer time by just the amount needed to encounter the destination moon at the desired place. In this respect, we recall (Table 4) that the synodic periods between moons are of a few days at most. On the other hand, the time spent in inter-moon space can be employed to perform observations of the environment of the E ring.

The results summarized in Table 5 and Figure 8 can be compared with those of [8] where a transfer from Dione to Enceladus through Tethys using resonant hopping takes 4.4 months and 28 m/s of velocity variation (to be imparted by impulsive maneuvers). Here, the equivalent transfer takes 150 days (5 months) and 660 m/s of ΔV which translates into 25 kg of propellant for a low-thrust maneuver. However, allowing for a longer time of flight enables extended observation of Tethys, an opportunity which a flyby does not offer.

We believe that the idea presented here deserves to be investigated further. In the future developments of this work, the simplified model of the circle-to-circle transfers will be replaced by an optimal control scheme that will vary the direction of thrust to connect the states at the CIs, and an in-depth analysis of the technologies needed to accomplish the type of mission outlined here will be conducted. This includes an investigation into the capabilities offered by the electrodynamic tether, which under well-defined conditions can be used to provide thrust. In conclusion, the tools developed and presented in this work can be employed to design a lunar cyclor of the Inner Large Moons of Saturn.

Acknowledgements

This research has been supported by Khalifa University of Science and Technology's internal grants CIRA-2018-85 and FSU-2018-07. The work of J. Peláez has been partially supported by MINECO/AEI, under Project ESP2017-87271-P, and FEDER/EU.

References

- [1] Committee on the Planetary Science Decadal Survey, Space Studies Board, Division on Engineering and Physical Engineering of the National Research Council of the National Academies, *Vision and Voyages for Planetary Science in the Decade 2013-2022*, The National Academies Press, Washington, DC, 2011.
- [2] Reh, K., Spilker, L., Lunine, J.I., Hunter Waite, J., et al., “Enceladus Life Finder: The search for life in a habitable moon”, *Proceedings of the 2016 IEEE Aerospace*, Big Sky, Montana, March 5-12, 2016.
- [3] Razzaghi, A.I., Simon-Miller A.A., Di Pietro, D., Spencer, J.R., et al., *Enceladus Flagship Mission Concept Study*, NASA Goddard Space Flight Center, August 29, 2007.
- [4] Buratti, B.J., Clark, R.N., Crary, F., Hansen, C.J., et al., “Cold cases: What we don’t know about Saturn’s Moons”, *Planetary and Space Science*, Vol. 155, 2018, pp. 41-49.
- [5] Dougherty, M.K and Spilker, L.J., “Review of Saturn’s icy moons following the Cassini mission”, *Reports on Progress in Physics*, Vol. 81, 2018, 065901.
- [6] Palacián, J.F., Lara, M. and Russell, R.P., “Mission design through averaging of perturbed Keplerian systems: the paradigm of an Enceladus orbiter”, *Celestial Mechanics and Dynamical Astronomy*, Vol. 108, No. 1, 2010, pp. 1-22.
- [7] Russell, R.P. and Strange, N.J., “Planetary Moon Cycler Trajectories”, *Journal of Guidance, Control, and Dynamics*, Vol. 32, No. 1, 2009, pp. 143-157.
- [8] Strange, N.J., Campagnola, S. and Russell, R.P., “Leveraging Flybys of Low Mass Moons to Enable an Enceladus Orbiter”, *Proceedings of the AAS/ALAA Astrodynamics Conference*, Pittsburgh, Pennsylvania, August 9-13, 2009.
- [9] Lantoine, G., Russell, R.P. and Campagnola, S., “Optimization of low-energy resonant hopping transfers between planetary moons”, *Proceedings of 60th International Astronautical Congress*, Daejeon, South Korea, October 12-16, 2009.
- [10] Brown, T.S., “Multi-body mission design in the Saturnian system with emphasis on Enceladus accessibility”, *Master of Science Degree Thesis*, Purdue University, 2008.
- [11] Geurts, K., Casaregola, C., Pergola, P. and Andrenucci, M., “Exploitation of the Three-Body Dynamics by Electric Propulsion for Outer Planetary Missions”, *Proceedings of the 43rd AIAA/ASME/SAE/ASEE Joint Propulsion Conference and Exhibit*, Cincinnati, Ohio, July 8-11, 2007.
- [12] Campagnola, S., Boutonnet, A., Martens, W., and Masters, A., “Mission design for the exploration of Neptune and Triton”, *IEEE Aerospace and Electronic Magazine*, Vol. 30, No. 7, 2015, pp. 6-17.
- [13] Szebehely, V., *Theory of orbits*, Academic Press, New York, 1967.
- [14] Siegel, C.L. and Moser, J.K., *Lectures on Celestial Mechanics*, Springer-Verlag, Berlin Heidelberg, 1971.

- [15] Parker, T.S. and Chua, L., *Practical Numerical Algorithms for Chaotic Systems*, Springer-Verlag, 1989.
- [16] Fantino, E. and Castelli, R., “Efficient design of direct low-energy transfers in multi-moon systems”, *Celestial Mechanics & Dynamical Astronomy*, Vol. 127, 2017, pp. 429-450, DOI: 10.1007/s10569-016-9733-9.
- [17] Roy, A.E., *Orbital Motion*, Third Edition, Adam Hilger, 1988.
- [18] Edelbaum, T.N., “Propulsion requirements for controllable satellites”, *ARS Journal*, Vol. 31 No. 8, 1961, pp. 1079-1089.
- [19] Van Noord, J.L., “Lifetime Assessment of the NEXT Ion Thruster”, *Proceedings of the 43rd AIAA/ASME/SAE/ASEE Joint Propulsion Conference and Exhibit*, Cincinnati, Ohio, July 8-11, 2007, paper AIAA 2007-5274.